Journal of the Geological Society, London, Vol. **164**, 2007, pp. 175–187. Printed in Great Britain.

Evidence for anoxia at the Ediacaran–Cambrian boundary: the record of redox-sensitive trace elements and rare earth elements in Oman

S. SCHRÖDER[1,2] & J. P. GROTZINGER[1,3]

[1]*Earth, Atmospheric and Planetary Sciences, Massachusetts Institute of Technology, 77 Massachusetts Avenue, Cambridge, MA 02139, USA*

[2]*Present address: Department of Geology, University of Johannesburg, Auckland Park 2006, Johannesburg, South Africa (e-mail: stefans@uj.ac.za)*

[3]*Present address: Division of Geological and Planetary Sciences, California Institute of Technology, Pasadena, CA 91125, USA*

Abstract: The Ediacaran–Cambrian boundary in Oman is characterized by a globally correlative negative $\delta^{13}C_{carb}$ excursion in platform carbonate rocks, and deposition of basinal organic-rich rocks. These observations may relate to the development of local, and possibly global, anoxia. We have studied redox-sensitive trace elements (TE) and REE from basinal and platform successions. Detrital input and authigenic element enrichment were the main factors controlling the record of TE and REE. Trace elements in the basin are enriched relative to crustal concentrations. In siliceous rocks, TE enrichment was decoupled from detrital input, suggesting authigenic concentration of TE under anoxic (possibly sulphidic) water column conditions. Trace elements and REE indicate higher detrital input in shales. Element enrichment was minimally influenced by detrital input in the platform carbonate rocks; it is strongest in the basal platform section, coincident with the carbon isotope excursion. The results suggest development of anoxia in a stagnant basinal water mass. Overturn or upward expansion of the deep water charged with TE and isotopically light C produced anoxia on the platform, and was probably related to development of the isotope excursion. These results are consistent with anoxia in boundary strata of Iran, and with the hypothesis of global anoxia at this time.

The Ediacaran–Cambrian transition is a key period for the understanding of the evolution of life and its relationship to biogeochemical changes. A large-magnitude negative carbon isotope excursion has long been recognized in close proximity to the Ediacaran–Cambrian boundary (e.g. Grotzinger *et al*. 1995; Bartley *et al*. 1998; Walter *et al*. 2000; Amthor *et al*. 2003). The excursion was preceded by a prolonged period with high burial rates of organic material (Grotzinger *et al*. 1995; Saylor *et al*. 1998). Burial led to ^{13}C enrichment in surface waters, as recorded in carbonate rocks, and caused accumulation of isotopically light CO_2 in basins (e.g. Knoll *et al*. 1996; Holser 1997*a*; Kimura *et al*. 1997). At the same time, heavy $\delta^{34}S$ in sulphate rocks indicates ^{34}S enrichment in surface waters and burial of reduced sulphur in organic-rich basin sediments (e.g. Walter *et al*. 2000; Schröder *et al*. 2004). These observations led previous workers to suggest anoxia for several Ediacaran–Cambrian boundary sections (e.g. Walter *et al*. 2000; Kimura & Watanabe 2001), but direct studies of redox conditions in this time interval are sparse. Overturn or simple expansion of an anoxic water mass could have delivered isotopically light CO_2 to shallow platform areas, thus affecting the shallow-water carbon isotope record (Knoll *et al*. 1996; Kimura *et al*. 1997; Bartley *et al*. 1998). However, the global or local nature of such conditions is still poorly constrained.

Firm radiometric ages and suitable facies development are major requirements for this kind of study. In the Ara Group of Oman, a negative carbon isotope excursion occurs in uranium-enriched platform carbonate rocks, which correlate with organic-rich shales and siliceous rocks (Mattes & Conway Morris 1990; Amthor *et al*. 2003). Organic biomarkers for chemoautotrophic bacteria, water stratification, and heavy $\delta^{34}S$ in platform evaporites suggest anoxic conditions in the basin (Grantham *et al*. 1987; Schröder *et al*. 2004; Amthor *et al*. 2005). The good age constraints for this succession (Amthor *et al*. 2003) and the availability of excellent sample material from hydrocarbon exploration wells allow a detailed study of redox conditions, environmental differences in platform and basin strata, and of how detrital input may have diluted the authigenic record of redox conditions (see Piper 1994). Samples along a platform-to-basin transect were selected for the analysis of redox-sensitive trace elements (TE) and REE. The results from this study are discussed, followed by a reconstruction of redox conditions at the time of deposition.

Geological setting

Age constraints and palaeogeography

The Ara Group was deposited between *c*. 550 Ma and 540 Ma (Fig. 1; Loosveld *et al*. 1996; Amthor *et al*. 2003). The basal age of *c*. 550 Ma is derived (Amthor *et al*. 2003) from correlation of a carbon isotope anomaly to a radiometrically dated section in Namibia (Saylor *et al*. 1998). An ash bed near the top of the Ara Group was dated at 542.0 ± 0.3 Ma (Fig. 1; Amthor *et al*. 2003). This horizon coincides with a prominent, globally correlative negative carbon isotope excursion, interpreted to mark the Ediacaran–Cambrian boundary in Oman (Fig. 1; Amthor *et al*. 2003).

These rocks accumulated in a series of basins in the interior of Oman, one being the South Oman Salt Basin (Fig. 2). During deposition of the Ara Group, the South Oman Salt Basin was subdivided in three palaeogeographical domains: two platform

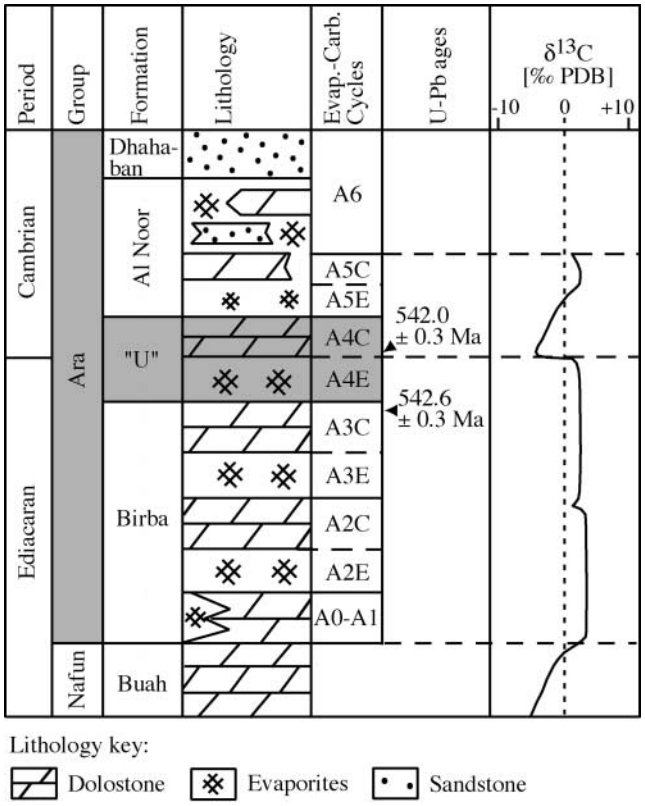


Fig. 1. Stratigraphy of the Ara Group in the South Oman Salt Basin (platform areas). The studied interval is highlighted in grey. Each Ara Group cycle contains an evaporitic unit (e.g. A4E) and a carbonate unit (e.g. A4C). Thicknesses are not to scale. The younger Ara Group ash bed coincides with a negative $\delta^{13}C$ anomaly (adapted from Loosveld *et al*. 1996; Amthor *et al*. 2003).

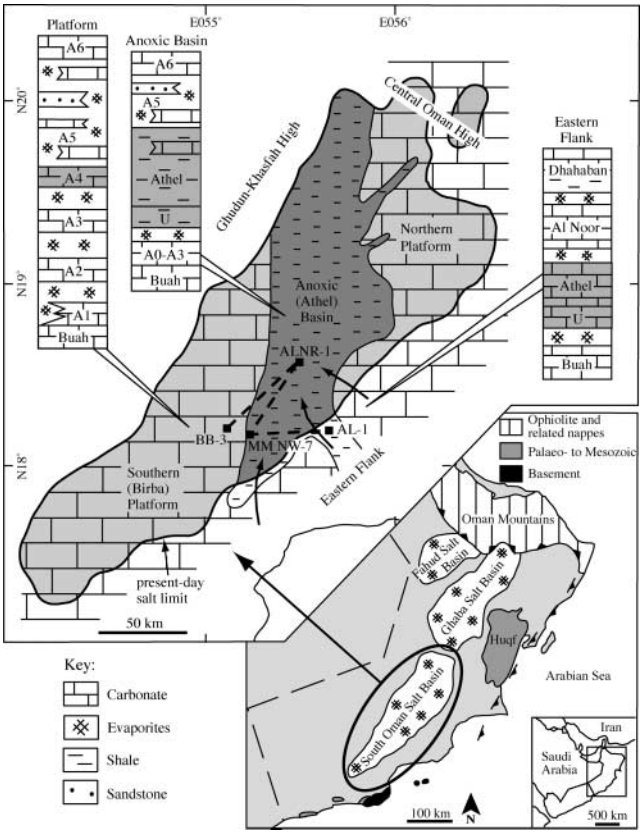


Fig. 2. Geological setting of the study area. The lower map shows the general geology of Oman (after Loosveld *et al*. 1996). The detailed setting of the South Oman Salt Basin is enlarged in the upper map. Individual stratigraphic columns are given for the Birba Platform, Athel Basin and the Eastern Flank. In each column, the studied interval is highlighted in grey. Arrows on the map illustrate the dominant sources of detrital sediment (see text). Black squares and the dashed line indicate wells and the cross-section in Figure 4a.

areas flanking a deep basin (Athel Basin; Fig. 2). Platform deposits consist of up to six tectono-eustatic evaporite–carbonate cycles (Figs 2 and 3). Evaporite rocks in each cycle are up to several hundred metres thick and were deposited in shallow salinas (Schröder *et al*. 2003). Carbonate units are 50–150 m thick and consist mainly of dolostone with smaller amounts of limestone (Fig. 3a; Schröder *et al*. 2005).

Platform deposits: A4E and A4C

The A4 carbonate unit (A4C) is present in drill core from the Birba Platform (Fig. 2), where it represents deposition on a muddy carbonate ramp (Fig. 3a; Mattes & Conway Morris 1990; Schröder *et al*. 2005). A flooding surface and the 542 Ma ash bed separate the underlying evaporite unit (A4E) from the A4C (Schröder *et al*. 2003). Carbonate deposition started with deeper-water laminated rocks that formed in an outer ramp environment (Fig. 3a and b). Organic content is usually *c*. 1 wt% total organic carbon (TOC), but locally exceeds 2 wt% TOC (Mattes & Conway Morris 1990). These rocks are overlain by middle ramp distal carbonate turbidites (Fig. 3a and c). Shallow subtidal cross-laminated carbonate rocks and microbialites occur at the top of the succession; very shallow deposits, including tidal facies, are absent (Fig. 3a; Schröder *et al*. 2005).

Chemostratigraphic studies have revealed several geochemical anomalies in the A4C. First, a negative carbon isotope excursion occurs at the base of the A4C and was dated at 542.0 ± 0.3 Ma (Amthor *et al*. 2003). Second, A4C rocks carry a strong gamma-ray signal that can be used for basin-wide correlation. The signal has two components: K enrichment associated with the ash bed and overall strong uranium enrichment throughout the A4C ($\leqslant$7 ppm; Mattes & Conway Morris 1990; Amthor *et al*. 2003).

Basinal deposits: U and Athel Formations

The thick evaporite units bracketing the A4C on the platform can be traced using seismic reflection data to the basin, where a succession, hundreds of metres thick, of organic-rich fine-grained siliciclastic, siliceous and carbonate rocks occurs between the evaporite units (Figs 2 and 4a). A strong gamma-ray signal and uranium enrichment in the lower part of the succession further substantiate correlation with the A4C (Fig. 4a). The basin rocks belong to the U and Athel Formations (Figs 2 and 4a; Amthor *et al*. 2005). In the basin centre, two transgressive shale units occur at the base and top of the succession: the U shale (equivalent to U Formation) and the Thuleilat shale (top of Athel Formation). Between them are unusual siliceous rocks of the Athel silicilyte, deposited during a highstand phase (Figs 2 and 4a; Amthor *et al*.

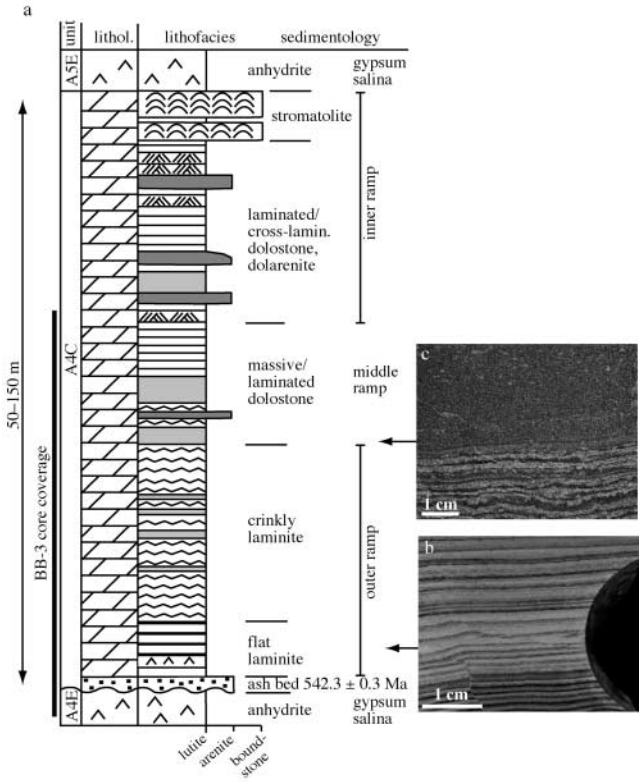


Fig. 3. (**a**) Typical sedimentary log of the A4 carbonate (A4C), showing the vertical succession of lithofacies and the environments. (**b**) Slabbed core sample of fine horizontal laminated carbonate (light grey) and anhydrite (dark grey) of the outer ramp (group 1 carbonate rocks). (**c**) Slabbed core sample of crinkly laminated organic-rich facies (bottom) overlain by massive carbonate rock of the middle ramp. This sample is characteristic for group 2 carbonate rocks (see text).

2005). Towards the Eastern Flank, the basin rocks pass laterally into platform carbonate rocks (Fig. 4a; Amthor *et al*. 2005).

The U shale is more than 80 m thick and has characteristic uranium enrichment. It consists of organic-rich mudstones and siltstones with strong gamma-ray and high-density well-log signals (Fig. 4a; Amthor *et al*. 2005).

The U shale grades upward to the Athel silicilyte (Fig. 4a), which is several hundred metres thick. A shift from low to high gamma-ray response defines lower and upper silicilyte (Fig. 4a). The unit consists of lutitic siliceous rocks with usually more than 80 wt% silica in the form of authigenic microcrystalline quartz (Amthor *et al*. 2005). Accessory minerals include illite, dolomite, magnesite, pyrite, apatite and zircon, whereas silt- and sand-sized detritus is rare (Amthor *et al*. 2005). A fine (>20 μm) horizontal, wavy and crinkly lamination is typical (Fig. 4b and c; Amthor *et al*. 2005).

Overlying the silicilyte rocks is the Thuleilat shale, which is up to 140 m thick and possesses a high gamma-ray response (Fig. 4a; Amthor *et al*. 2005). Rocks are petrographically similar to those of the U shale, but they contain more carbonate and lack the uranium enrichment.

Total organic carbon contents of all units averages 3–4 wt% TOC, but the U shale and Thuleilat shale often have higher TOC values (up to 9 wt% TOC) than the Athel silicilyte (Alixant *et al*. 1998). Organic material is finely disseminated, and occurs in intercrystalline porosity and stylolites (Amthor *et al*. 2005).

Basin reconstructions indicate that water depths exceeded 100–150 m in most of the Athel Basin (Amthor *et al*. 2005). The basin has a steep, possibly faulted western margin along the Birba Platform (Figs 2 and 4a). The Eastern Flank formed the gentle eastern slope of the basin (Fig. 2), whereas a number of fault-bounded intrabasinal highs occurred in the central and western Athel basin (Amthor *et al*. 2005). They were sites of either non-deposition or deposition of shallow-water A4C rocks. The silicilyte thickens from the Eastern Flank basinwards, whereas the detrital content and gamma-ray signal strength decrease in the same direction (Fig. 4a; Amthor *et al*. 2005). The thicknesses of the two shale units decrease basinwards. These observations suggest dominant detrital input from the Eastern Flank, whereas the intrabasinal highs did not act as sources of significant sediment input (Fig. 2).

Diagenesis

The platform carbonate rocks form structural compartments that are entirely enclosed within evaporite rocks, and diagenetic modification included mainly early dolomitization and formation of diagenetic evaporites (Mattes & Conway Morris 1990). Geochemical signatures of these carbonate rocks are generally regarded as close to their original values (Mattes & Conway Morris 1990; Schröder 2000).

In shales and silicilyte, early diagenesis included porosity occlusion by pyrite formation, compaction and silica cementation. These processes occurred at temperatures below *c*. 60 °C (Amthor *et al*. 2005). Subsequently, brittle fracturing affected the rocks, and fractures were cemented by quartz, apatite, magnesite and barite at temperatures around and above 100 °C (Amthor *et al*. 2005). Some late halite cementation was observed.

Geochemical background

Detrital input

The total concentration of a given element in sediments is usually composed of three independent fractions: detrital, biogenic and hydrogenous (i.e. derived from seawater; Piper 1994; Piper & Isaacs 1995). Monitoring the detrital fraction is necessary to assess the enrichment of redox-sensitive elements relative to their detrital (i.e. crustal) component. Incompatible elements with short residence times in seawater are ideally suited for this, because they will be transferred almost quantitatively to the sediment, and should thus closely reflect the composition of the continental crust (Taylor & McLennan 1985; Webb & Kamber 2000). Some of these elements are dependent on source area and grain size (see Taylor & McLennan 1985; Johnson & Grimm 2001). The present study uses Th, rather than Al_2O_3, as a monitor for detrital input, because Th is largely independent of factors such as grain size, and Al data were not available. Thorium concentrations will be compared with concentrations of Ti, Zr and Y/Ho. Diagenetic modification of Ti, Th and Zr concentrations is unlikely in carbonate rocks, because these elements are associated mainly with non-carbonate components (Veizer 1983*a*).

Rare earth elements

Rare earth elements do not have a redox chemistry, except Ce and Eu (McLennan 1989). Siliciclastic detritus is the main source of sedimentary REE, and REE profiles in shales will reflect REE contents in Post-Archaean Average Shale (PAAS), which represents average crustal composition (Taylor & McLennan 1985). In

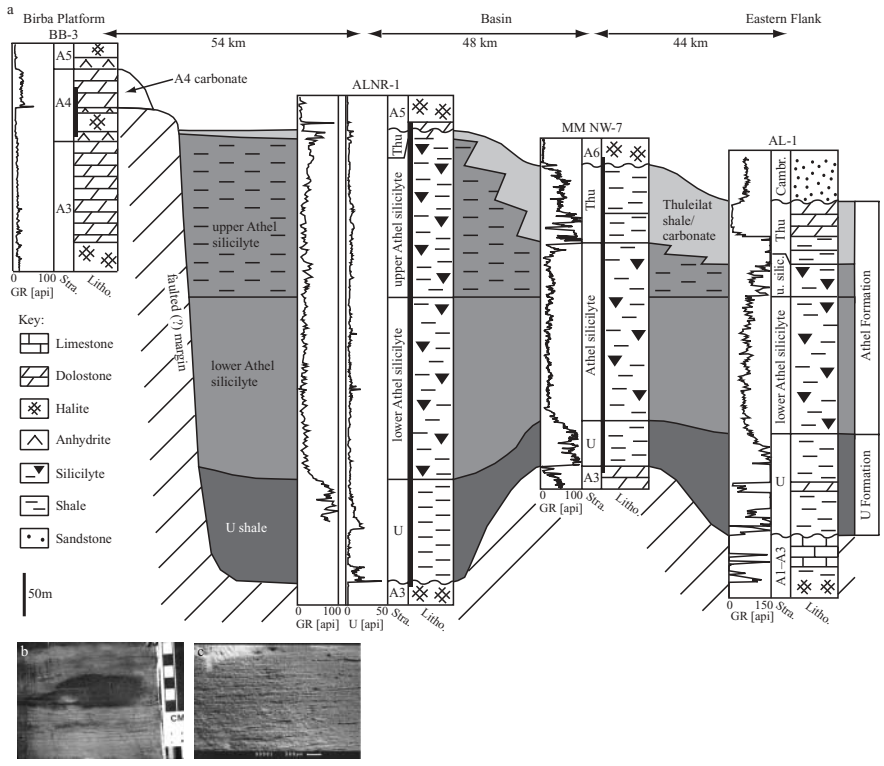


Fig. 4. (**a**) Cross-section from the Birba Platform through the central Athel Basin to the Eastern Flank (indicated by dashed line in Fig. 2). Stratigraphic columns show lithology, gamma-ray (GR), uranium response (where available) and stratigraphic subdivisions for the wells studied. The black bars next to the stratigraphic subdivisions indicate studied sections in each well; well AL-1 has been added as a representative for the Eastern Flank, but was not studied in detail. (**b**) Slabbed core of silicilyte with the characteristic fine crinkly lamination (compare with Fig. 3b). Scale bar in centimetres. (**c**) SEM image of silicilyte, showing the fine lamination and porosity. Scale bar represents 300 μm.

contrast, authigenic sediments with negligible detrital influence can potentially preserve seawater REE composition (McLennan 1989).

Anomalies of Ce are of particular interest in this study, because they can record redox conditions in the overlying water column and during early diagenesis (German & Elderfield 1990; Holser 1997*b*). However, anomalous La/Nd ratios can cause erroneous calculation of Ce anomalies, which are not related to Ce geochemistry. Anomalies are given as Ce/Ce*, where Ce* denotes Ce concentration in PAAS (McLennan 1989). True Ce anomalies are monitored in a plot of Ce/Ce* v. Pr/Pr* (Bau & Dulski 1996).

Redox-sensitive trace elements

In this study, 'anoxic' denotes conditions when oxygen was probably minimal to essentially absent. Anoxia–euxinia develops in the presence of HS^-. The term 'dysoxic' refers to conditions varying between anoxic and oxic, or when oxygen levels were relatively low but constant (see Wignall & Myers 1988).

Manganese is enriched in Mn-oxides under oxic conditions. Reducing diagenesis produces soluble Mn^{2+}, which diffuses away from the site of reduction (Morford *et al*. 2001). Reduced Mn can be reprecipitated in the presence of O_2, or it forms Mn-carbonate where alkalinity is high. Although Mn is commonly depleted in sediments undergoing anoxic diagenesis, it is also evident that element recycling across redox boundaries can be important (Calvert & Pedersen 1996; Morford *et al*. 2001).

Vanadium is frequently used together with Cr to monitor redox conditions in the nitrate reduction zone. Elements are immobilized as hydroxides close to the lower boundary (V) and upper boundary (Cr) of the nitrate reduction zone, respectively (Jones & Manning 1994; Piper 1994). Denitrification characterizes dysoxic conditions (Froelich *et al*. 1979). Commonly, V is associated with organic matter, but some fraction may be bound in silicate minerals as well (Jones & Manning 1994). Because of analytical problems with Cr, only V concentrations were considered in this study.

Rivers are the only significant source of uranium to the oceans (Klinkhammer & Palmer 1991). The element is immobilized in sediments with active sulphate reduction by diffusion of U^{6+} to sediments, reduction to U^{4+}, followed by adsorption and precipitation (Cochran *et al*. 1986; Klinkhammer & Palmer 1991; Jones & Manning 1994; Morford *et al*. 2001). Additional uranium may be supplied by direct precipitation from an anoxic water mass (Piper & Isaacs 1995). Diagenetic re-oxidation has been suggested to cause uranium loss from sediments (e.g. Cochran *et al*. 1986), but downward diffusion of mobilized uranium is more likely (e.g. Thomson *et al*. 1993). Authigenic uranium is calculated as $U_{aut} = U_{tot} - Th/3$, with Th/3 as an estimate of the detrital uranium fraction (Wignall & Myers 1988; Jones & Manning 1994).

Molybdenum has very high seawater concentrations relative to crustal values and can record seawater conditions even with significant clastic input (Piper 1994; Crusius *et al*. 1996). Immobilization occurs when ambient HS^- activity exceeds threshold values, causing particle-reactive behaviour of Mo and scavenging by organic material and/or Fe-bearing particles (e.g. sulphides; Helz *et al*. 1996; Zheng *et al*. 2000). Molybdenum scavenging seems to occur close to the sediment–water interface and in the water column, and enrichment is thought to coincide with euxinic conditions (Crusius *et al*. 1996; Lyons *et al*. 2003).

Samples and methods

Sample selection

Samples were collected from three wells along a transect from the platform (well BB-3) through the intermediate (well MM NW-7) to the deep basin (well ALNR-1) (Figs 2 and 4a). Material from the platform

well covers the basal two-thirds of the A4C (Fig. 3a). The basin wells provided samples from the entire basin succession (Fig. 4a).

For the platform well, several grams of samples were obtained directly from core with a hand drill. Cuttings were used for the basin wells. About 1–5 g of material were obtained by handpicking clean, individual chips based on visual inspection. Further cleaning involved an air duster and 5% HCl to remove superficial stains and dust. Chips were then ground in a ceramic mortar.

Preparation and analysis

Powdered samples were dried overnight at 450 °C; sample weight before and after this process was recorded to allow correction of element concentrations for the loss on ignition. Dried sample (about 50–100 mg) was subsequently weighed and transferred to 15 ml Teflon screw-cap vials. Dissolution of samples was done in several steps with acid addition. In each step, the solution was left on a hotplate for 1–10 h before evaporating it gently to dryness. The following acids were used subsequently: (1) a mix of 1 ml 8N HNO_3 and 2 ml concentrated HF; (2) 2 ml 8N or concentrated HNO_3 (depending on amount of sample and residue after the first dissolution step); (3) 2 ml 8N HNO_3 (repeated once); (4) sample was taken up in 6 ml 8N HNO_3 without subsequent evaporation; (5) if residue was left after step (4), the supernatant solution was decanted, and the remaining solution was then evaporated and dissolved again in 4 ml 8N HNO_3 before combining the two solutions. Residue occurred only in a small number of samples and probably consisted of organic material, based on visual inspection. It made up $\leqslant$0.1 wt% of the liquid and a correction was applied to these samples. The final solution was transferred into polyethylene tubes, centrifuged and diluted for analysis with de-ionized water. The analytical solutions had a HNO_3 concentration of 1–3% to match HNO_3 concentration in washing and tuning solutions used during analysis. Dilution factors of analytical solutions ranged from 2000 to 100 000.

Standard samples were prepared in an identical fashion from reference materials of a known and certified composition. The following reference materials were used: (1) shales and silicilyte: MAG-1, SCo-1, SDO-1 and SGR-1, which are shale samples issued by the USGS; (2) carbonate: DWA-1, a dolomite standard distributed by the Université de Liège. Because of the lack of a suitable sulphate reference material, standard DWA-1 was also used for anhydrite analyses.

A VG Plasmaquad II inductively coupled plasma mass spectrometry (ICP-MS) system was used for all analyses. Samples were introduced using an autosampler tray. The analytical setup involved both internal drift monitors (to correct for instrument drift) and external drift monitors (to correct for mass-dependent sensitivity variations) (Eggins *et al*. 1997). All unknown sample and standard solutions were spiked with an internal standard containing Be, In and Bi at a concentration of 4 ppb. External drift monitor solutions, prepared from the standard solutions, were analysed repeatedly during an individual measurement run, usually every 5–8 samples. Procedural blank samples were analysed in each run. The raw data were corrected for internal drift, mass-dependent sensitivity variations, and blank levels using the computer application Tangiers© developed for MIT.

Repeated standard runs allowed estimation of the analytical reproducibility. In the shale and silicilyte standards, most elements varied by 5–6%. The element variability was generally higher in the carbonate standard, and most elements varied by $\pm$10%. Molybdenum generally showed variability exceeding these values (shale/silicilyte 2–41%, carbonate >50%).

Estimates of the analytical accuracy are based on comparisons between the measured concentrations in standards and published concentrations. Differences relative to the USGS standards are 7–15%, but most elements are within 10% of the published value. However, the 1σ error margins given by the USGS commonly exceed errors of this study. For the carbonate standards, an accuracy of 6–12% is a good estimate; this is generally better than the published error margins. Titanium analyses had relatively poor accuracy in some runs (shale/silicilyte 5–72%, carbonate 4–41%). Measured values for Mn and Mo commonly remained below detection limits as a result of low peak-to-background ratios. Detection limits were calculated separately for each run.

Data presentation

Data are reported in parts per million (ppm). To interpret excess enrichment of elements relative to their detrital fraction in the basin samples, element concentrations were plotted together with element concentrations in PAAS, which represents average crustal composition and is used as a baseline for rocks deposited under oxic conditions (Taylor & McLennan 1985; Sageman *et al*. 2003). The ratio TE/Th was compared in samples (TE/Th_{sample}) and in PAAS (TE/Th_{PAAS}) to highlight fluxes of a particular element relative to its detrital fraction (e.g. Davis *et al*. 1999; Kato *et al*. 2002; Sageman *et al*. 2003). The approach for the carbonate platform samples was identical; however, average carbonate composition as given by Turekian & Wedepohl (1961) was used as a baseline (except for Mn, which is essentially controlled by diagenesis; Banner & Hanson 1990). The REE were normalized to their concentrations in PAAS (Taylor & McLennan 1985). Profiles of REE can be further characterized by enrichments of light, middle and heavy REE (LREE, MREE and HREE, respectively), and these were calculated according to Holser (1997*b*), Webb & Kamber (2000) and Shields & Stille (2001).

Results

Analytical results are available online at http://www.geolsoc.org.uk/SUP18256. A hard copy can be obtained from the Society Library. A descriptive summary of the stratigraphic trends and the cross-correlation between parameters is provided in Table 1. The section below highlights the main observations in platform and basin samples.

Platform

The detrital parameters are generally depleted relative to average carbonate concentrations (Fig. 5a, Table 1). Cross-correlation between the various parameters is moderate to good (Fig. 5d–f).

According to their REE profiles and bulk REE concentrations ($\sum$REE), platform samples can be arranged into three distinct groups (Fig. 6a and Table 1): (1) volcanic ash samples; (2) the basal four samples of the A4C, representing outer ramp deposition (group 1 carbonate rocks; see Fig. 3b); (3) the remainder of carbonate samples (group 2 carbonate rocks). All samples are depleted in $\sum$REE relative to PAAS (Fig. 6a and Table 1). As a very broad trend, $\sum$REE decreases up section (Fig. 6a), but it does not correlate with the detrital monitors (Fig. 6b). True positive Ce anomalies occur in samples from the basal A4C (Fig. 6c). Several platform samples display a marked positive Eu anomaly (Fig. 6a). This anomaly, however, is an analytical artefact related to Ba interferences during analysis, because there is a good correlation between Eu/Eu* and Ba/Nd (see data in the Supplementary Publication; Shields & Stille 2001).

Absolute TE concentrations vary significantly with stratigraphic position. Enrichment relative to average carbonate is a common feature of all parameters, except Mn, and the enrichment is most pronounced in the basal A4C samples (Fig. 7 and Table 1).

Basin

Both wells show similar trends of detrital parameters with stratigraphic depth. Concentrations tend to be close to PAAS values in the U shale and Thuleilat shale, but they are strongly depleted in the silicilyte samples (Fig. 5b and c; Table 1). Concentrations of these elements are tightly clustered in silicilyte samples, but are more scattered in shale samples (Fig. 5d–f).

Basin samples present consistently flat REE profiles with minor variation. Samples from the shales have $\sum$REE close to

Table 1. *Description of main results*

Geochemical parameter	Platform: well BB-3	Basin: well ALNR-1	Basin: well MM NW-7
Detrital proxies: Th	Depleted relative to average carbonate; peak in ash samples, decreasing up section (Fig. 5a)	Near crustal values in U shale and Thuleilat shale, depleted in silicilyte; increasing up section to Thuleilat shale (Fig. 5b and c)	
Detrital proxies: Ti	Depleted relative to average carbonate; peak in ash samples, ± constant up section (Fig. 5a)	Same as Th above (Fig. 5b and c)	
Detrital proxies: Zr	Same as Ti above	Same as Th and Ti above	
REE profile and ∑REE	∑REE decreases up section (Fig. 6a); (1) ash: ∑REE *c*. half of PAAS, slight HREE enrichment (Fig. 6a); (2) group 1: ∑REE *c*. two orders of magnitude < PAAS, strong HREE depletion, slight MREE enrichment (Fig. 6a); (3) group 2: ∑REE *c*. three orders of magnitude < PAAS, flat profile	Mostly flat profiles with minor variation; silicilyte and chert samples are almost indistinct and tend towards slight HREE enrichment (Fig. 8a); ∑REE in U shale and Thuleilat shale similar to PAAS, *c*. one order of magnitude smaller in silicilyte (Fig. 8a) LREE enrichment in U shale	HREE enrichment most pronounced in Thuleilat shale
REE: Ce anomaly	True positive Ce anomaly in two group 1 carbonate samples ($Ce/Ce^* = 1.09–1.10$) (Fig. 6c)	True negative Ce anomalies common ($Ce/Ce^* = 0.57–0.93$), but no systematic variation with lithology or stratigraphic position (Fig. 8c); single silicilyte sample of MM NW-7 with true positive Ce anomaly ($Ce/Ce^* = 1.23$) (Fig. 8c)	
Redox: Mn	Increases gradually up section (Fig. 7a); Mn/Th increases sharply at base of A4C, flattens out at values above average carbonate, again increases in middle ramp (Fig. 7c); no correlation with detrital parameters (Fig. 9a)	Concentrations < PAAS, tend to be higher and more variable in the shale units than in silicilyte (Fig. 10a); no vertical trends of Mn/Th, ratio smaller than or equal to Mn/Th in PAAS (Fig. 10b); no correlation with detrital parameters (Fig. 9a)	Peak at 2700–2705 m correlates with higher carbonate content
Redox: V	Peak near base of A4C, dropping to ⩽5 ppm up section (Fig. 7b); peak concentrations exceed average carbonate; V/Th increases sharply at base of A4C, flattens out at values above average carbonate (Fig. 7c); no correlation with detrital parameters (Fig. 9c)	Silicilyte concentrations similar to or slightly > PAAS, V is strongly enriched in shale units (Fig. 10c); V/Th enriched above PAAS throughout succession (Fig. 10d); no correlation with detrital parameters, but silicilyte samples tend to be more tightly clustered (Fig. 9b)	
Redox: U/Th	Increases up section (Fig. 7a), ratio above average carbonate (except ash samples)	Enriched > PAAS throughout succession, peak near base of succession, two intervals of pronounced enrichment in silicilyte (Fig. 11a)	Mostly below PAAS, increasing through silicilyte to prominent peak near top of unit, which is strongly enriched > PAAS
Redox: U_{aut}	Highly variable, values ⩽5 ppm (Fig. 7b); no correlation with detrital parameters (Fig. 9b)	Enriched > PAAS throughout succession, peaks in basal U shale and in Thuleilat, increasing through upper silicilyte (Fig. 11a); no correlation with detrital parameters, but silicilyte samples tend to be more tightly clustered (Fig. 9b)	
Redox: Mo	Absolute values and Mo/Th similar in behaviour to V, below detection limit above base; no correlation with detrital parameters (Fig. 9d)	Mo/Th > PAAS; no correlation with detrital parameters, but silicilyte samples tend to be more tightly clustered (Fig. 9d) No vertical trends of absolute concentrations; Mo/Th strongly enriched > PAAS in lower silicilyte (Fig. 11c)	High absolute concentrations in shale units, drop in silicilyte (Fig. 11b); no vertical trends of Mo/Th, few samples near top of silicilyte have Mo/Th < PAAS

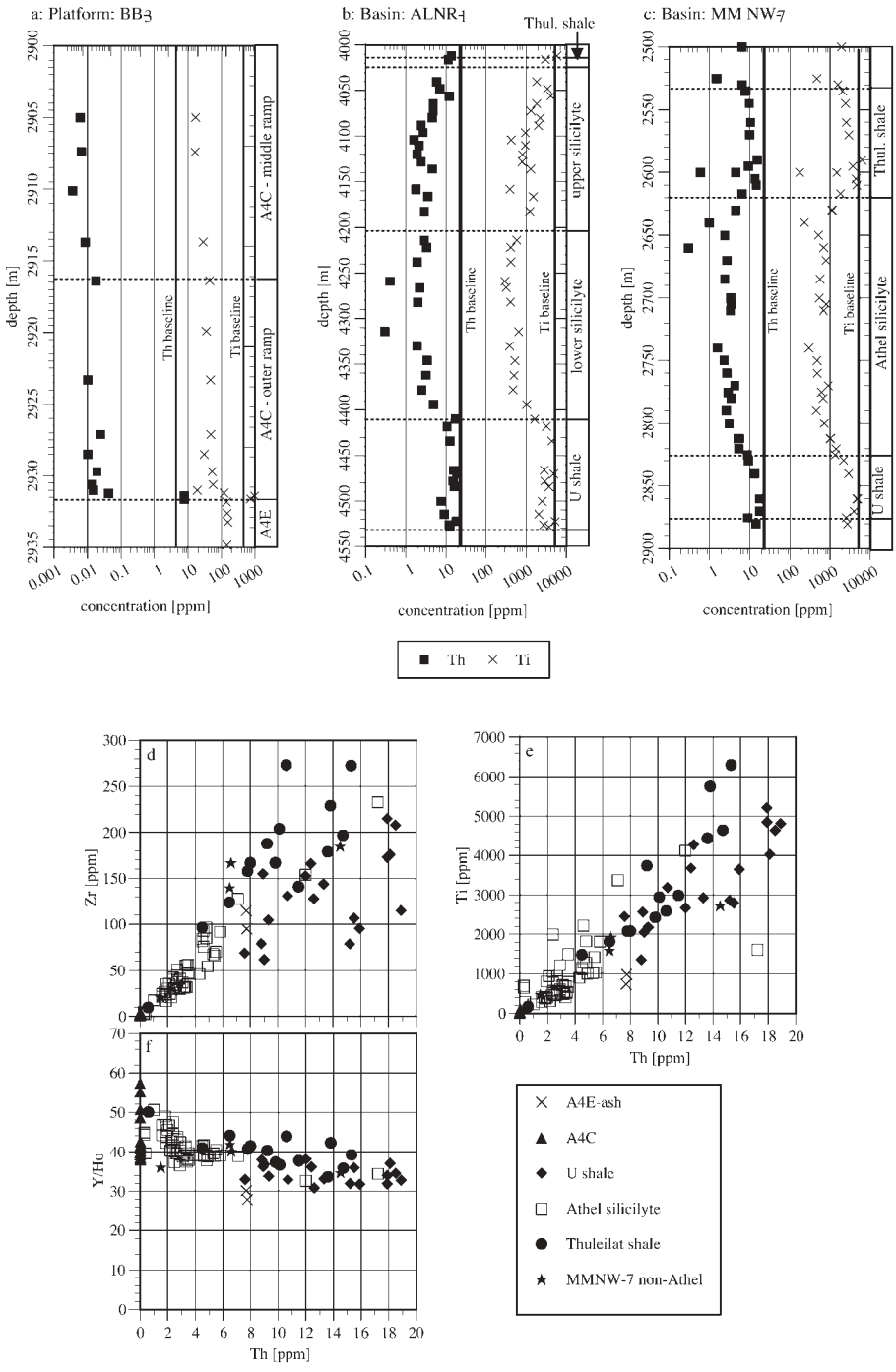


Fig. 5. (**a**–**c**) Record of detrital parameters Th and Ti with depth in the three wells. Stratigraphic subdivisions are given for each well. The grey bars and grey bars with horizontal ticks mark the baseline concentrations of Th and Ti in average carbonate (well BB-3) and Post-Archaean Average Shale (PAAS; basin wells), respectively. (**d**–**f**) Plots of the detrital parameter Th v. Zr, Ti and Y/Ho, respectively.

PAAS, whereas ∑REE is about one order of magnitude smaller in silicilyte rocks (Fig. 8a and Table 1). The ∑REE of silicilyte samples correlates relatively well with Ti concentration, but such a direct relationship does not hold for U shale and Thuleilat shale samples (Fig. 8b). Instead, these samples scatter above the regression curve established for silicilyte samples. True Ce anomalies are present; however, there is no systematic variation with either lithology or stratigraphic position (Fig. 8c). The observed Eu anomalies are an analytical artefact related to Ba interferences (Fig. 8a).

No correlation of TE with detrital monitors is evident, but the silicilyte values are clustered at the lower end of the concentration spectrum, whereas variability is much higher in the shales (Fig. 9). Redox trace elements show variable stratigraphic trends (Table 1). Concentrations of Mn are mostly below crustal levels in both wells, but they are highest in the U shale and Thuleilat shale (Fig. 10a and b). In contrast, all other parameters tend to be enriched to variable degrees relative to PAAS (Figs 10c, d and 11). The enrichment usually is most pronounced in the U shale and Thuleilat shale (e.g. V and U_{aut}, Figs 10c, and 11a) or in the lower silicilyte (e.g. Mo/Th, Fig. 11c). Comparisons with data from other anoxic basins show a similar, if not higher enrichment in Oman (Figs 10c and 11a, b).

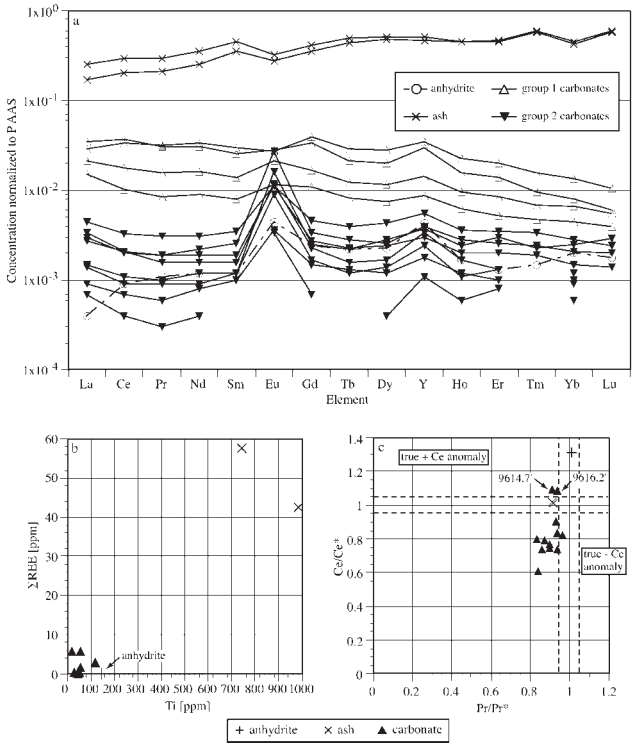


Fig. 6. REE in platform samples. (**a**) REE profiles. It should be noted that, as a general trend, ∑REE of carbonates decreases up section. (**b**) Plot of Ti v. ∑REE. (**c**) Diagram after Bau & Dulski (1996) to monitor true Ce anomalies.

Data interpretation and discussion

Platform

Detrital input. Low trace element concentrations suggest minimal detrital influence, consistent with earlier petrographic studies (Fig. 5a; Mattes & Conway Morris 1990; Schröder *et al*. 2005).

Rare earth elements. The three distinct groups of REE patterns correspond to different sources of REE (Fig. 6a). First, HREE enrichment and the Y/Ho ratio of *c*. 28 in the two ash samples are typical of a volcanic source (Taylor & McLennan 1985). Their ∑REE is close to crustal values. The flat REE pattern of the group 2 samples is essentially identical to that of shales, but with the low ∑REE characteristic for ancient marine carbonate rocks (Fig. 6b; Taylor & McLennan 1985; Banner *et al*. 1988). Lastly, group 1 samples share the relatively low, carbonate-like ∑REE, but with HREE depletion and MREE enrichment that could suggest diagenetic modification (see Taylor & McLennan 1985; Shields & Stille 2001).

None of the carbonate rocks studied here have seawater REE signature, but instead, group 2 samples clearly reflect detrital influence. Even minute amounts of detrital minerals can swamp the seawater signature in carbonate systems, because the REE concentrations are much higher in detritus than in seawater (Taylor & McLennan 1985; Webb & Kamber 2000). Detrital influence is supported by Y/Ho ratios <44 in several samples, which indicate the presence of at least a small detrital fraction (see Webb & Kamber 2000). On the other hand, the lack of correlation between Y/Ho ratios and Th concentrations (Fig. 5f) suggests the presence of other factors influencing REE patterns in platform samples (e.g. diagenesis).

The MREE enrichment and HREE depletion of group 1 samples are similar to patterns ascribed by Shields & Stille (2001) to diagenetic REE remobilization. Normally, concentrations of REE in carbonate rocks are very high relative to natural

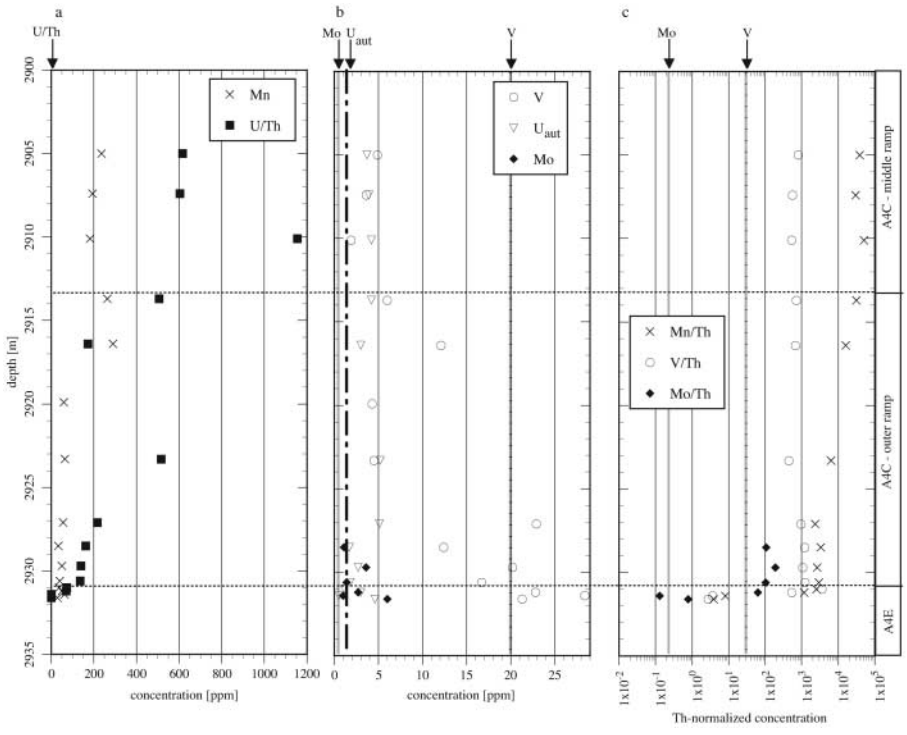


Fig. 7. Redox-sensitive trace element record in the platform well BB-3. (**a**) Manganese and U/Th ratio. The U/Th ratio in average carbonate (1.3; Turekian & Wedepohl 1961) is indicated at the top. (**b**) Concentrations of V, U_{aut} and Mo. The respective concentrations in average carbonate are given along the top. (**c**) Concentrations of Mn, V and Mo normalized to Th. The respective values in average carbonate, except for Mn, are indicated along the top.

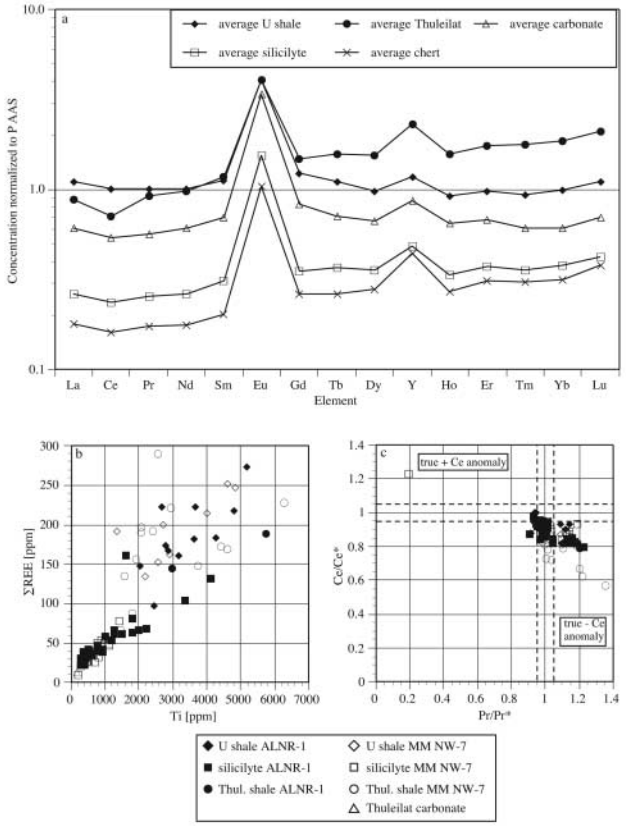


Fig. 8. REE in basin samples. (**a**) REE profiles. The average for the U shale does not include samples that were almost pure chert; instead, they are grouped under average chert for this study (see also text). (**b**) Plot of Ti v. ∑REE. Samples from both wells are considered separately, as are carbonate-rich samples of well MM NW-7. (**c**) Diagram after Bau & Dulski (1996) to monitor the presence of true Ce anomalies.

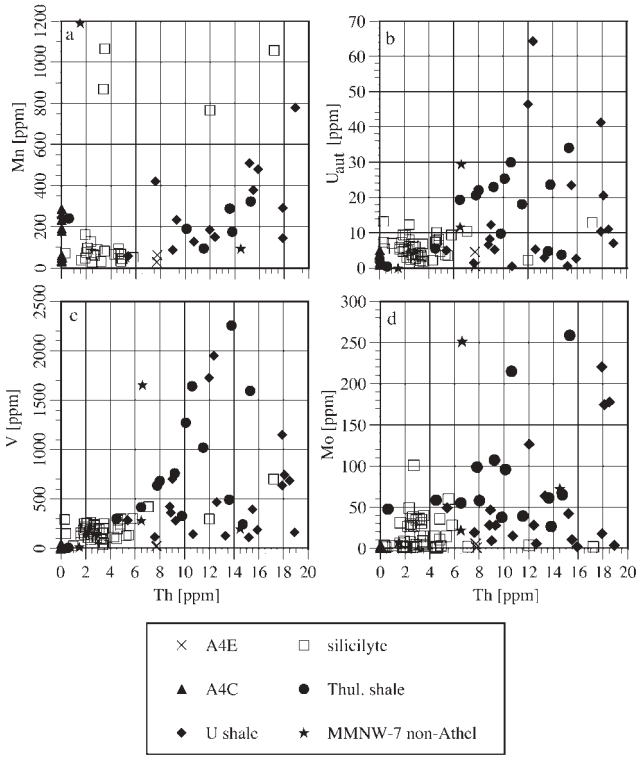


Fig. 9. Cross plots of Th as detrital monitor v. (**a**) Mn concentration, (**b**) authigenic uranium, (**c**) V concentration (**d**) and Mo concentration in samples from all three wells.

fluids, requiring very high diagenetic fluid–rock ratios to change REE concentrations (Banner *et al*. 1988). Earlier studies of Ara Group dolomite rocks have demonstrated low fluid–rock ratios during diagenesis and preservation of marine geochemical signatures (Mattes & Conway Morris 1990; Schröder 2000; Amthor *et al*. 2003). On a decimetre to metre scale, however, diagenetic remobilization of REE and enrichment could have occurred, and the relatively REE-enriched ash bed just below the group 1 samples would represent the most likely REE source.

The true positive Ce anomaly in two platform samples, from the basal portion of the A4C, could indicate anoxic conditions in the overlying water column and/or during early diagenesis (Fig. 6c). These samples have the highest ∑REE of all A4C samples, and primary Ce concentrations can be modified during significant diagenetic REE enrichment and exchange with pore waters (German & Elderfield 1990; Shields & Stille 2001). Even if Ce anomalies can be demonstrated to be primary, they provide a time-integrated record of redox conditions (German & Elderfield 1990).

Redox-sensitive trace elements. Manganese concentrations in platform samples are more likely to be the result of diagenetic processes than to be a reflection of depositional conditions, because Mn is strongly involved in carbonate diagenesis (Veizer 1983*b*; Banner & Hanson 1990). This includes redox variation and water–rock interaction, and the results of the two processes are usually difficult to separate (Banner & Hanson 1990).

The peak of V, near the base of the A4C and exceeding average carbonate concentration, is indication of redox-controlled enrichment (Fig. 7b). It is unrelated to detrital proxies (Fig. 9c), but may be related to a higher organic content (see Jones & Manning 1994). The lower values in the upper part of the succession suggest dysoxic conditions, although the Th-normalized values remain above the baseline (Fig. 7c).

The up-section increase of U/Th in A4C samples is a combination of two parallel trends: (1) decreasing Th concentration throughout the core; (2) increase of uranium in the basal part of the succession, followed by largely constant values (Figs 5a and 7a). Thus, at least the base of the A4C is characterized by strong enrichment of uranium above average carbonate levels, which also is evident in U_{aut} (Fig. 7b). These data indicate oxygen-deficient conditions in sediments and possibly the water column at least at the base of the A4C, but possibly occurring throughout A4C deposition. However, some of the uranium enrichment could be related to uranium bound to organic material (see Klinkhammer & Palmer 1991).

The high values of Mo and Mo/Th_{sample} in the basal part of the A4C may be indicative of euxinic conditions at least in the sediments (e.g. Crusius *et al*. 1996; Lyons *et al*. 2003). The lack of data from the upper part of the core precludes further interpretations of the Mo data (Fig. 7c).

Basin

Detrital input. Moderate to good cross-correlation between the various detrital parameters suggests that these parameters can be used interchangeably (Fig. 5d–f). Data for detrital input to the basinal rocks correlate with the petrographic observation that the

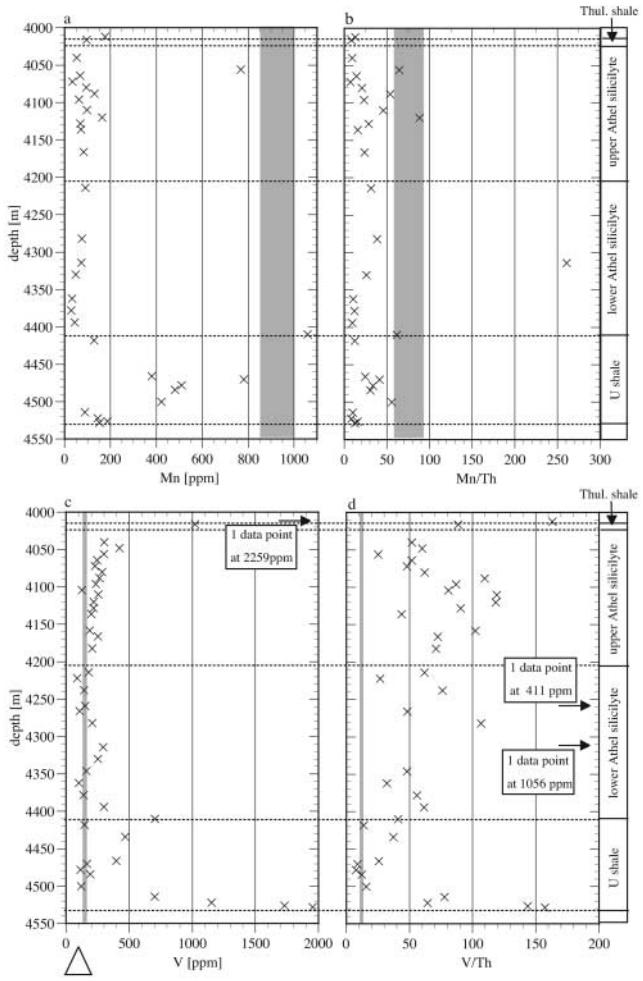


Fig. 10. Trace element data for well ALNR-1. Grey bars in all figures mark the respective values in Post-Archaean Average Shale (PAAS). (**a**) Absolute concentrations of Mn. (**b**) Mn/Th. (**c**) Absolute concentrations of V. Triangle at bottom indicates average V concentration in anoxic sediments (Kato *et al*. 2002). (**d**) V/Th.

shales are typical clastic units, whereas the Athel silicilyte is a unit formed largely by authigenic silica precipitation. Elements Ti and Th reach crustal concentrations only in the shale units (Fig. 5b and c). Although the silicilyte is strongly depleted in all detrital proxies, the increase of these elements throughout the upper silicilyte of well ALNR-1 mirrors the higher gamma-ray signal and correlates with increased detrital input (Figs 4a and 5b; Amthor *et al*. 2005). Not only was detrital input generally higher in the shales, but the poor correlation between Th and Zr in these units also could indicate variable sources for the two elements and detrital input (Fig. 5d).

Rare earth elements. The flat REE pattern of the majority of samples is identical to that of shales (Fig. 8a; Taylor & McLennan 1985). Total REE concentrations in U shale and Thuleilat shale are similar to those of PAAS and therefore closely reflect crustal composition (Fig. 8a and b). The lower $\sum$REE of silicilyte and in particular the chert-rich samples reflects stronger dilution of the clastic signal by the precipitation of chert. Nevertheless, the good correlation of detrital parameters and $\sum$REE for all samples is evidence that detrital input dominated the REE system of the basin sediments (Fig. 8b). The slight preferential enrichment of HREE in Thuleilat shale, silicilyte and chert samples, and the true negative Ce anomalies in some of these samples could reflect a relict seawater signal (Fig. 8a and c; McLennan 1989; Holser 1997*b*). However, it has been pointed out above that primary REE signals are easily modified during diagenesis (German & Elderfield 1990; Shields & Stille 2001), and a negative anomaly does not necessarily indicate oxidation of Ce at the place of deposition itself, but somewhere in the basin (M. Bau, pers. comm.). A similar argument for diagenetic overprint can be made for the single silicilyte sample with a true positive Ce anomaly (Fig. 8c). Thus, the value of these Ce anomalies for palaeoredox interpretations remains ambiguous.

Redox-sensitive trace elements. Depletion of Mn relative to PAAS in basin samples suggests removal of reduced Mn from sediments, which can occur under a range of oxygen-deficient conditions from dysoxic to euxinic (Froelich *et al*. 1979). Reduced soluble Mn^{2+} may form solid Mn carbonate (e.g. Pratt *et al*. 1991), undergo oxidation in the presence of oxic bottom waters (Calvert & Pedersen 1996), or diffuse away from the site

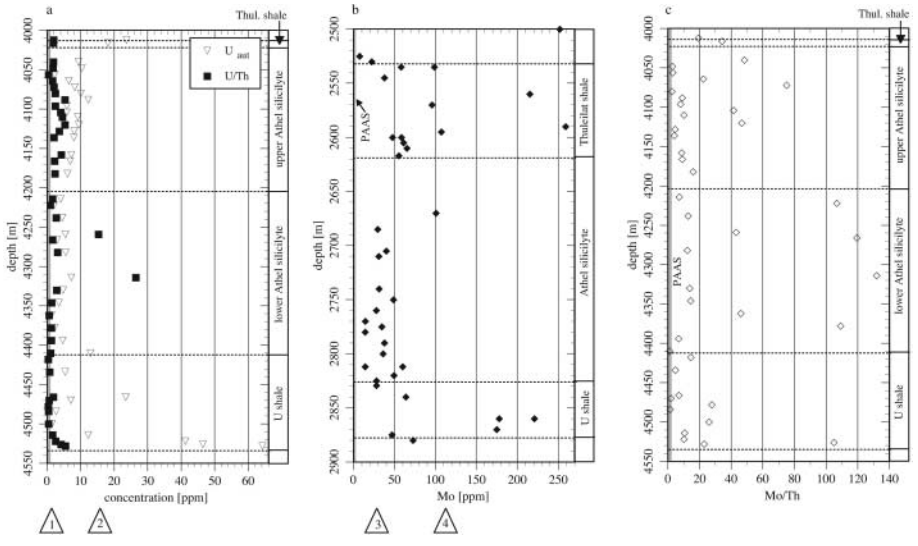


Fig. 11. (**a**) Authigenic uranium concentrations and U/Th ratio in well ALNR-1. The Post-Archaean Average Shale (PAAS) value of U/Th is indicated by the grey bar, whereas the baseline for U_{aut} is zero. Triangles at bottom indicate averages in various anoxic sediments: (1) U_{aut} (Kato *et al*. 2002); (2) U/Th (Jones & Manning 1994). (**b**) Absolute Mo concentrations and PAAS baseline (grey bar) in well MM NW-7. Triangles at bottom indicate average Mo concentration in various anoxic sediments (3, Taylor & McLennan 1985; 4, Lyons *et al*. 2003). (**c**) Values of Mo/Th and PAAS baseline (grey bar) in well ALNR-1.

of reduction. The last process leaves sediments permanently depleted in Mn, and Mn concentrations in sediments are a function of Mn contents in the detrital fraction delivered to the basin (Calvert & Pedersen 1996). Although this is broadly consistent with the observed variation of Mn with Th (Fig. 9a), the absence of a well-defined correlation between the two elements, and the much higher scatter of data from the shale units indicate additional controls. The extent of Mn depletion is a function of the duration of oxygen deficiency (Calvert & Pedersen 1996), and Mn loss may have been less efficient during deposition of the U shale and Thuleilat shale. For example, sediment conditions may have been permanently or temporarily dysoxic in these units. In addition, Mn could be bound to carbonate, consistent with the observation that some samples with a significant carbonate component also have elevated Mn concentrations (Table 1). A contribution of Mn from hydrothermal sources is unlikely, because even the samples least influenced by detrital input lack a hydrothermal REE signature.

Anoxic conditions and V accumulation in sediments are indicated by the strong enrichment of the element relative to PAAS. Detrital sources of V and variations in organic matter contents may influence the V record in the shale units (see Jones & Manning 1994). However, there is no correlation of V with detrital input (Fig. 9c). After correction for detrital fluxes, enrichment is similar throughout the succession, pointing to a strong redox control on V accumulation.

The enrichment of both uranium parameters above crustal levels in most of the basin samples is evidence for sulphate-reducing conditions in sediments, but possibly extending into the water column. Sulphate reduction is consistent with $\delta^{34}S$ and biomarker data, and the high sulphur contents of oils derived from the silicilyte (Grantham *et al*. 1987; Schröder *et al*. 2004). The similarity of stratigraphic trends of U_{aut} and TOC (Alixant *et al*. 1998) indicates a first-order association with organic matter, similar to observations from other localities (e.g. Cochran *et al*. 1986; Klinkhammer & Palmer 1991). Nevertheless, detrital input in the U shale may have affected U_{aut}, and to a lesser extent U/Th (Figs 9b and 11a), although no direct correlation exists between U_{aut} and Th. Shale samples, which have the highest bulk detrital fraction, also show strongest variability of U_{aut} (Fig. 9b). Rivers are the only significant source of uranium to the oceans (Klinkhammer & Palmer 1991), and variations in the uranium contents of this source will affect the amount of uranium buried in sediments.

Molybdenum enrichment above PAAS is similar to concentrations in other anoxic basins (Fig. 11b). Although Mo enrichment can occur in sulphidic sediments under a dysoxic or oxic water column, the high concentrations observed in this study are more consistent with the presence of HS^- in the water column (see Lyons *et al*. 2003; Meyers *et al*. 2005). The stronger variability in the shale units suggests some relationship with detrital influence and the elevated TOC in these units (Fig. 9d). Molybdenum scavenging strongly depends on the reactivity and type of organic material, and on HS− concentrations, which will be affected by the availability of organic material and sulphate for bacterial sulphate reduction. The association with organic material may, however, lead to overestimation of the reducing conditions in the environment (Tribovillard *et al*. 2004).

Implications for redox chemistry of the South Oman Salt Basin

The platform record may have been modified by carbonate diagenesis, and this would have affected mainly Mn and uranium concentrations. Concentrations of the other TE and REE are largely controlled by any detrital fraction in carbonate rocks and by sedimentary redox conditions (see Banner & Hanson 1990). Thus, enrichment of TE used in this study above average carbonate concentrations is particularly good evidence for the development of anoxia at least at the base of the A4C (possibly sulphidic, based on the Mo record). Lower absolute concentrations in the upper part of the studied section indicate dysoxic or even oxic conditions, whereas the normalized data point to continuous anoxia in the sampled section. It remains unclear, however, whether these conditions were restricted to sediments or extended into the water column.

All redox proxies for the basin point to anoxic conditions in sediments throughout the entire succession. The high Mo enrichment suggests that bottom waters could have been sulphidic. Other factors such as detrital input and organic material played a major role in modifying the authigenic signal, and this is visible in the U shale and Thuleilat shale record. For example, rivers are the main source for some of the elements analysed in this study (e.g. uranium). Organic material is strongly linked to the accumulation of Mo, uranium and V (Klinkhammer & Palmer 1991; Helz *et al*. 1996). In turn, detrital input will dilute organic matter fluxes and affect burial and remineralization of organic material, and provide nutrients that control organic productivity. The Mn record remains more ambiguous, but includes the possibility of more dysoxic intervals and the influence of detrital and carbonate-bound Mn in shale units. The current sampling interval of 5 m does not allow resolution of high-frequency redox variations that have been observed in some modern reducing basins (e.g. Murphy *et al*. 2000), and that could have generated dysoxic intervals during deposition of U shale and Thuleilat shale (see Piper 1994). In summary, this study has recognized some of the universal factors governing deposition of organic-rich facies and authigenic element enrichment, such as the relative roles of immobilization and remineralization of TE, as well as availability of organic material and the dilution effects of terrigenous clastic material (e.g. Wignall 1994; Sageman *et al*. 2003).

Our results are consistent with earlier interpretations of the deeper parts of the South Oman Salt Basin as an anoxic stratified basin, based on biomarker and sulphur isotopes (Peters *et al*. 1995; Schröder *et al*. 2004; Amthor *et al*. 2005). Data from this study provide direct geochemical evidence that these rocks were deposited under anoxic conditions, including the possibility of sulphidic bottom water. Additionally, the data support the hypothesis of anoxia in shallower platform areas during A4 deposition. Anoxic deep water generally requires a stagnant, commonly stratified water body, where circulation is too sluggish to bring sufficient oxygen to the deep water mass, although recent studies suggest that even short-term variations in O_2 content do not preclude a long-term record of anoxia (e.g. Murphy *et al*. 2000). Modelling results for the end-Permian anoxia suggest alternation between sluggish haline circulation and more vigorous thermal circulation (see Zhang *et al*. 2001). If haline circulation and anoxia dominate over the time span of oscillation, the time-averaged rock record will indicate anoxic conditions. Periods with higher sediment input could be associated with stronger (thermally driven) circulation and lead to, on average, rather dysoxic conditions, which may explain the elevated Mn concentrations in the Thuleilat and U shales. On the other hand, the saline conditions in the South Oman Salt Basin would have been ideally suited to cause relatively stable salinity stratification in the basin. The notion of relatively low, but nevertheless increasing atmospheric O_2 concentrations during the

Neoproterozoic (Canfield 1998) further supports development of stable stratification in basins of this time.

In either case, the anoxic lower water mass would have been enriched in H_2S, HCO_3^-, CO_2, P and isotopically light carbon as a result of organic matter remineralization (e.g. Knoll *et al*. 1996). The evidence for anoxia in the platform succession can be linked to either overturn or upward expansion of this anoxic water. The negative carbon isotope excursion is estimated to last 1 Ma at most (Grotzinger *et al*. 1995; Amthor *et al*. 2003), and it coincides with transgression in the South Oman Salt Basin. These observations are more readily explained by upward expansion of an anoxic water mass during transgression than by short-lived overturn. The data suggest a causal link between overturn–expansion of the anoxic water mass charged with isotopically light carbon, and the negative carbon isotope excursion in platform rocks (see Kimura *et al*. 1997; Bartley *et al*. 1998). Other scenarios for the excursion include methane release (Walter *et al*. 2000) and phytoplankton extinction (Hsü *et al*. 1985), although the latter is inconsistent with mass balance calculations (Bartley *et al*. 1998).

High $\delta^{34}S$ in Ara Group sulphate rocks and positive $\delta^{13}C_{carb}$ record elevated burial rates of reduced sulphur and organic carbon in all older stratigraphic levels of the Ara Group (Amthor *et al*. 2003; Schröder *et al*. 2004). Although this will result in increased oxygenation of surface waters, oxygen will not necessarily be transferred to bottom waters, because of: (1) trapping of O_2 above the chemocline in the absence of vigorous circulation (see above); (2) consumption by organic matter respiration; (3) the low solubility of O_2 in the expected saline bottom water. As a result, anoxia could have built up gradually over time in the South Oman Salt Basin. Data for redox-sensitive parameters from the other Ara Group cycles are needed to further constrain the frequency of anoxic conditions during Ara Group deposition. The current study and results from Iran (Kimura & Watanabe 2001) provide firm evidence that anoxia developed at least regionally at the Ediacaran–Cambrian boundary. The water mass in the South Oman Salt Basin must have had a connection to the open ocean. The carbon isotope anomaly and marine fossils *Cloudina* and *Namacalathus* occur worldwide in a stratigraphic position that can be correlated to Oman (Amthor *et al*. 2003), and Br concentrations in Ara Group evaporite rocks indicate a marine rather than a continental source (Schröder *et al*. 2003). Therefore, although oceanic water masses could have been modified in the partly restricted basins of the Persian Gulf area, global oceanic anoxia at this time was possible.

Conclusions

Ediacaran–Cambrian boundary strata in Oman consist of: (1) platform carbonate rocks, which record the boundary negative carbon isotope excursion and were dated at 542.0 ± 0.3 Ma (U–Pb zircon age); (2) a correlative basin succession of black shales and organic-rich siliceous rocks ('silicilyte'). Previous studies of sulphur isotopes and organic biomarkers have indicated anoxic conditions in the deeper parts of the basin, which may be related to global anoxia at this time. The present study uses redox-sensitive trace elements (TE) and REE to investigate redox conditions in platform and basin rocks.

Detrital input and authigenic element enrichment are the main factors controlling the record of these parameters. In the basin, input of detrital material was highest in shale units. Profiles of REE are typical for shales and record average crustal composition. Trace elements throughout the succession are enriched relative to average crustal composition. In silicilyte samples, the enrichment of TE was decoupled from detrital input, suggesting true authigenic concentration of redox-sensitive elements. Additional factors may have governed element concentrations in the shale units: (1) element concentration coupled to the detrital fraction and/or organic matter (e.g. U, Mo); (2) intervals with dysoxic conditions and less efficient removal of Mn; (3) association of Mn with carbonate. The platform record shows only minimal detrital influence, and strong TE enrichment in the basal part of the succession, coincident with the carbon isotope excursion.

The results of this study are consistent with the development of water column anoxia–euxinia in a salinity-stratified basin. The Ediacaran–Cambrian boundary in Oman coincided with overturn or upward expansion of the trace element- and CO_2-charged anoxic water mass, causing oxygen depletion in platform strata and leading to the negative carbon isotope shift. The bulk of the data indicate that regionally anoxia of even shallow seawater occurred at this time. The isochronous correlation of the global carbon isotope anomaly at the Ediacaran–Cambrian boundary suggests that this event also may have occurred globally.

Petroleum Development Oman, LLC gave financial and logistical support and permission to publish these results. Financial support was provided by NASA grant NAG5-9445 to J.P.G., and by the 'Gemeinsames Sonderprogramm III von Bund und Ländern', distributed through the German Academic Exchange Service (DAAD), to S.S. Helpful comments by D. Fike on an earlier version and thoughtful reviews by T. Lyons and an anonymous reviewer greatly enhanced the manuscript. The authors wish to thank B. Bergquist, E. Boyle, C. Colonero, S. Higgins, S. Huang, R. Kayser, J. Morford and R. Summons for valuable help in the laboratory.

References

Alixant, J.-L., Frewin, N., Nederlof, P. & Al-Ruwehy, N. 1998. Characterisation of the Athel silicilyte source rock/reservoir: petrophysics meets geochemistry (abstract). *In: Society of Professional Well Log Analysts 39th Annual Logging Symposium*. 1–14.

Amthor, J.E., Grotzinger, J.P., Schröder, S., Bowring, S.A., Ramezani, J., Martin, M.W. & Matter, A. 2003. Extinction of *Cloudina* and *Namacalathus* at the Precambrian–Cambrian boundary in Oman. *Geology*, **31**, 431–434.

Amthor, J.E., Ramseyer, K., Faulkner, T. & Lucas, P. 2005. Stratigraphy and sedimentology of a chert reservoir at the Precambrian–Cambrian Boundary: the Al Shomou Silicilyte, South Oman Salt Basin. *GeoArabia*, **10**, 89–122.

Banner, J.L. & Hanson, G.N. 1990. Calculation of simultaneous isotopic and trace element variations during water–rock interaction with applications to carbonate diagenesis. *Geochimica et Cosmochimica Acta*, **54**, 3123–3137.

Banner, J.L., Hanson, G.N. & Meyers, W.J. 1988. Rare earth element and Nd isotopic variations in regionally extensive dolomites from the Burlington&-Keokuk Formation (Mississippian): implications for REE mobility during carbonate diagenesis. *Journal of Sedimentary Petrology*, **58**, 415–432.

Bartley, J.K., Pope, M., Knoll, A.H., Semikhatov, M.A. & Petrov, P.Y. 1998. A Vendian–Cambrian boundary succession from the northwestern margin of the Siberian Platform: stratigraphy, palaeontology, chemostratigraphy and correlation. *Geological Magazine*, **135**, 473–494.

Bau, M. & Dulski, P. 1996. Distribution of yttrium and rare-earth elements in the Penge and Kuruman iron-formations, Transvaal Supergroup, South Africa. *Precambrian Research*, **79**, 37–55.

Calvert, S.E. & Pedersen, T.F. 1996. Sedimentary geochemistry of manganese: implications for the environment of formation of manganiferous black shales. *Economic Geology*, **91**, 36–47.

Canfield, D.E. 1998. A new model for Proterozoic ocean chemistry. *Nature*, **396**, 450–453.

Cochran, J.K., Carey, A.E., Sholkovitz, E.R. & Surprenant, L.D. 1986. The geochemistry of uranium and thorium in coastal marine sediments and sediment pore waters. *Geochimica et Cosmochimica Acta*, **50**, 663–680.

Crusius, J., Calvert, S., Pedersen, T.F. & Sage, D. 1996. Rhenium and molybdenum enrichments in sediments as indicators of oxic, suboxic and sulfidic conditions of deposition. *Earth and Planetary Science Letters*,

145, 65–78.

Davis, C., Pratt, L., Sliter, W., Mompart, L. & Murat, B. 1999. Factors influencing organic carbon and trace metal accumulation in the Upper Cretaceous La Luna Formation of the western Maracaibo Basin, Venezuela. *In:* Barrera, E. & Johnson, C.C. (eds) *Evolution of the Cretaceous Ocean–Climate System*. Geological Society of America, Special Papers, **332**, 203–230.

Eggins, S.M., Woodhead, J.D. & Kinsley, L.P.J. *et al*. 1997. A simple method for the precise determination of ⩾40 trace elements in geological samples by ICPMS using enriched isotope internal standardisation. *Chemical Geology*, **134**, 311–326.

Froelich, P.N., Klinkhammer, G.P. & Bender, M.L. *et al*. 1979. Early oxidation of organic matter in pelagic sediments of the eastern equatorial Atlantic: suboxic diagenesis. *Geochimica et Cosmochimica Acta*, **43**, 1075–1090.

German, C.R. & Elderfield, H. 1990. Application of the Ce anomaly as a paleoredox indicator: the ground rules. *Paleoceanography*, **5**, 823–833.

Grantham, P.J., Lijmbach, G.W.M., Posthuma, J., Hughes Clark, M.W. & Willink, R.J. 1987. Origin of crude oils in Oman. *Journal of Petroleum Geology*, **11**, 61–80.

Grotzinger, J.P., Bowring, S.A., Saylor, B.Z. & Kaufman, A.J. 1995. Biostratigraphic and geochronologic constraints on early animal evolution. *Science*, **270**, 598–604.

Helz, G.R., Miller, C.V., Charnock, J.M., Mosselmans, J.F.W., Pattrick, R.A.D., Garner, C.D. & Vaughan, D.J. 1996. Mechanisms of molybdenum removal from the sea and its concentration in black shales: EXAFS evidence. *Geochimica et Cosmochimica Acta*, **60**, 3631–3642.

Holser, W.T. 1997a. Geochemical events documented in inorganic carbon isotopes. *Palaeogeography, Palaeoclimatology, Palaeoecology*, **132**, 173–182.

Holser, W.T. 1997b. Evaluation of the application of rare-earth elements to paleoceanography. *Palaeogeography, Palaeoclimatology, Palaeoecology*, **132**, 309–323.

Hsü, K.J., Oberhänsli, H., Gao, S., Chen, H. & Krähenbühl, U. 1985. Strangelove ocean before the Cambrian explosion. *Nature*, **316**, 809–811.

Johnson, K.M. & Grimm, K.A. 2001. Opal and organic carbon in laminated diatomaceous sediments: Saanich Inlet, Santa Barbara Basin and the Miocene Monterey Formation. *Marine Geology*, **174**, 159–174.

Jones, B. & Manning, D.A.C. 1994. Comparison of geochemical indices used for the interpretation of palaeoredox conditions in ancient mudstones. *Chemical Geology*, **111**, 111–129.

Kato, Y., Nakao, K. & Isozaki, Y. 2002. Geochemistry of Late Permian to Early Triassic pelagic cherts from southwest Japan: implications for an oceanic redox change. *Chemical Geology*, **182**, 15–34.

Kimura, H. & Watanabe, Y. 2001. Oceanic anoxia at the Precambrian–Cambrian boundary. *Geology*, **29**, 995–998.

Kimura, H., Matsumoto, R., Kakuwa, Y., Hamdi, B. & Zibaseresht, H. 1997. The Vendian–Cambrian $\delta^{13}C$ record, North Iran: evidence for overturning of the ocean before the Cambrian Explosion. *Earth and Planetary Science Letters*, **147**, E1–E7.

Klinkhammer, G.P. & Palmer, M.R. 1991. Uranium in the oceans: where it goes and why. *Geochimica et Cosmochimica Acta*, **55**, 1799–1806.

Knoll, A.H., Bambach, R.K., Canfield, D.E. & Grotzinger, J.P. 1996. Comparative earth history and late Permian mass extinction. *Science*, **273**, 452–457.

Loosveld, R., Bell, A. & Terken, J. 1996. The tectonic evolution of interior Oman. *GeoArabia*, **1**, 28–51.

Lyons, T.W., Werne, J.P., Hollander, D.J. & Murray, R.W. 2003. Contrasting sulfur geochemistry and Fe/Al and Mo/Al ratios across the last oxic-to-anoxic transition in the Cariaco Basin, Venezuela. *Chemical Geology*, **195**, 131–157.

Mattes, B.W. & Conway Morris, S. 1990. Carbonate/evaporite deposition in the Late Precambrian–Early Cambrian Ara Formation of Southern Oman. *In:* Robertson, A.H.F., Searle, M.P. & Ries, A.C. (eds) *The Geology and Tectonics of the Oman Region*. Geological Society, London, Special Publications, **49**, 617–636.

McLennan, S.M. 1989. Rare earth elements in sedimentary rocks: influence of provenance and sedimentary processes. *In:* Lipin, B.R. & McKay, G.A. (eds) *Geochemistry and Mineralogy of Rare Earth Elements*. Mineralogical Society of America, Reviews in Mineralogy, **21**, 169–200.

Meyers, S. R., Sageman, B. B. & Lyons, T. W. 2005. Organic carbon burial rate and the molybdenum proxy: theoretical framework and application to Cenomanian–Turonian oceanic anoxic event 2. *Paleoceanography*, **20**, PA2002, doi:10.1029/2004PA001068.

Morford, J.L., Russell, A.D. & Emerson, S. 2001. Trace metal evidence for changes in redox environment associated with the transition from terrigenous clay to diatomaceous sediment, Saanich Inlet, BC. *Marine Geology*, **174**, 355–369.

Murphy, A.E., Sageman, B.B., Hollander, D.J., Lyons, T.W. & Brett, C.E. 2000. Black shale deposition and faunal overturn in the Devonian Appalachian basin: clastic starvation, seasonal water-column mixing, and efficient biolimiting nutrient-recycling. *Paleoceanography*, **15**, 280–291.

Peters, K.E., Clark, M.E., Das Gupta, U., McCaffrey, M.A. & Lee, C.Y. 1995. Recognition of an Infracambrian source rock based on biomarkers in the Baghewala-1 oil, India. *AAPG Bulletin*, **79**, 1481–1494.

Piper, D.Z. 1994. Seawater as the source of minor elements in black shales, phosphorites and other sedimentary rocks. *Chemical Geology*, **114**, 95–114.

Piper, D.Z. & Isaacs, C.M. 1995. Minor elements in Quaternary sediments from the Sea of Japan: a record of surface-water productivity and intermediate-water redox conditions. *Geological Society of America Bulletin*, **107**, 54–67.

Pratt, L.M., Force, E.R. & Pomerol, B. 1991. Coupled manganese and carbon-isotopic events in marine carbonates at the Cenomanian–Turonian boundary. *Journal of Sedimentary Petrology*, **61**, 370–383.

Sageman, B.B., Murphy, A.E., Werne, J.P., Ver Straeten, C.A., Hollander, D.J. & Lyons, T.W. 2003. A tale of shales: the relative roles of production, decomposition, and dilution in the accumulation of organic-rich strata, Middle–Upper Devonian, Appalachian basin. *Chemical Geology*, **195**, 229–273.

Saylor, B.Z., Kaufman, A.J., Grotzinger, J.P. & Urban, F. 1998. A composite reference section for terminal Proterozoic strata of southern Namibia. *Journal of Sedimentary Research*, **68**, 1223–1235.

Schröder, S. 2000. *Reservoir quality prediction in Ara Group carbonates of the South Carbonate Platform, South Oman Salt Basin*. PhD thesis, University of Bern.

Schröder, S., Schreiber, B.C., Amthor, J.E. & Matter, A. 2003. A depositional model for the terminal Neoproterozoic–Early Cambrian Ara Group evaporites in south Oman. *Sedimentology*, **50**, 879–898.

Schröder, S., Schreiber, B.C., Amthor, J.E. & Matter, A. 2004. Stratigraphy and environmental conditions of the terminal Neoproterozoic–Cambrian Period in Oman: evidence from sulphur isotopes. *Journal of the Geological Society, London*, **161**, 489–499.

Schröder, S., Grotzinger, J.P., Amthor, J.E. & Matter, A. 2005. Carbonate deposition and hydrocarbon reservoir development at the Precambrian–Cambrian boundary: the Ara Group in South Oman. *Sedimentary Geology*, **180**, 1–28.

Shields, G. & Stille, P. 2001. Diagenetic constraints on the use of cerium anomalies as palaeoseawater redox proxies: an isotopic and REE study of Cambrian phosphorites. *Chemical Geology*, **175**, 29–48.

Taylor, S.R. & McLennan, S.M. 1985. *The Continental Crust: its Composition and Evolution*. Blackwell, Oxford.

Thomson, J., Higgs, N.C., Croudace, I.W., Colley, S. & Hydes, D.J. 1993. Redox zonation of elements at an oxic/suboxic boundary in deep-sea sediments. *Geochimica et Cosmochimica Acta*, **57**, 579–595.

Tribovillard, N., Riboulleau, A., Lyons, T.W. & Baudin, F. 2004. Enhanced trapping of molybdenum by sulfurized marine organic matter of marine origin in Mesozoic limestones and shales. *Chemical Geology*, **213**, 385–401.

Turekian, K.K. & Wedepohl, K.H. 1961. Distribution of the elements in some major units of the Earth's crust. *Geological Society of America Bulletin*, **72**, 175–192.

Veizer, J. 1983a. Trace elements and isotopes in sedimentary carbonates. *In:* Reeder, R.J. (ed.) *Carbonates: Mineralogy and Geochemistry*. Mineralogical Society of America, Reviews in Mineralogy, **11**, 265–300.

Veizer, J. 1983b. Chemical diagenesis of carbonates: theory and application of trace element technique. *In:* Arthur, M.A., Anderson, T.F., Kaplan, I.R., Veizer, J. & Land, L.S. (eds) *Stable Isotopes in Sedimentary Geology*. SEPM Short Course Notes, **10**, 3.1–3.100.

Walter, M.R., Veevers, J.J., Calver, C.R., Gorjan, P. & Hill, A.C. 2000. Dating the 840–544 Ma Neoproterozoic interval by isotopes of strontium, carbon, and sulfur in seawater, and some interpretative models. *Precambrian Research*, **100**, 371–433.

Webb, G.E. & Kamber, B.S. 2000. Rare earth elements in Holocene reefal microbialites: a new shallow seawater proxy. *Geochimica et Cosmochimica Acta*, **64**, 1557–1564.

Wignall, P.B. 1994. *Black Shales*. Clarendon, Oxford.

Wignall, P.B. & Myers, K.J. 1988. Interpreting benthic oxygen levels in mudrocks: a new approach. *Geology*, **16**, 452–455.

Zhang, R., Follows, M.J., Grotzinger, J.P. & Marshall, J. 2001. Could the Late Permian deep ocean have been anoxic? *Paleoceanography*, **16**, 317–329.

Zheng, Y., Anderson, R.F., van Geen, A. & Kuwabara, J. 2000. Authigenic molybdenum formation in marine sediments: a link to pore water sulfide in the Santa Barbara Basin. *Geochimica et Cosmochimica Acta*, **64**, 4165–4178.

Received 21 February 2005; revised typescript accepted 22 June 2006.
Scientific editing by John Marshall